# Enhancing natural gas dehydration performance using electrospun nanofibrous sol-gel coated mixed matrix membranes

**Seyed Jalil Poormohammadian\*, Parviz Darvishi\*,†, and Abdol Mohammad Ghalambor Dezfuli\*\***

*Department of Chemical Engineering, School of Engineering, Yasouj University, Yasouj, Iran
**Physics Department, Faculty of Science, Shahid Chamran University of Ahvaz, Ahvaz, Iran
(*Received 9 April 2018 • accepted January 14, 2019*)

**Abstract**−The dehydration process of natural gas was investigated by mixed matrix membranes (MMM), which were fabricated by electrospinning and sol-gel coating methods. Silica and titania nanoparticles (NPs) were incorporated into the polymer matrix via sol-gel method. The fabricated MMMs were characterized by field emission electron microscopy (FESEM), X-ray diffraction (XRD) and Fourier transform infrared spectroscopy (FTIR). Dehydration tests were carried out for wet pure methane and natural gas streams individually. The effects of different process parameters, including feed and sweep gas flow rates, moisture content in the feed, feed pressure and other hydrocarbons in the feed were investigated. The prepared electrospun nanofibrous supports (ESNS) have smaller fiber diameters in comparison to previously reported works, and with regard to the commercially available materials, contribute to higher water vapor permeation. The results showed that by increasing the feed pressure from 2.5 to 15 bar for the membranes without NPs, the permeance of methane and water vapor was decreased by 8.2 and 29%, respectively. It was also observed that the permeance of heavier hydrocarbons in Pebax 1657 membrane is higher than methane, leading to the increase of $H_2O/CH_4$ selectivity and the loss of heavier hydrocarbons. Finally, determining the resistances of the support and selective layers based on the existing empirical relations demonstrated that the total resistance to water vapor transmission had decreased by 75.2% using ESNS instead of microporous supports (MPS). In addition, the contribution of support layer resistances was decreased from 67% in MPS membranes to less than 30% in ESNS ones.

Keywords: Natural Gas Dehydration, Mixed Matrix Membranes, Electrospinning, Sol-gel Method, Water Vapor Transition

## INTRODUCTION

The presence of water vapor in natural gas is responsible for major problems in gas transfer pipelines, such as corrosion, hydrate formation, pneumatic systems destruction, gas heating-value reduction, high-pressure drops, and reduction in gas transmission efficiency. These phenomena damage the equipment of compression units and pipelines. To meet pipeline specifications, natural gas should not contain water vapor more than 7 lb/MMscf [1].

Natural gas can be dehydrated by different methods, including absorption [2,3], adsorption [4], refrigeration and supersonic [5], and membrane permeation [6]. Traditionally, Triethylene glycol (TEG) units have been widely used to remove water from industrial gas streams. Glycol dehydration faces increasing environmental restrictions for volatile organic compounds (VOCs) emitted by the unit, hazardous air pollutants (BTEX) and NOx from the regeneration reboiler. Besides, the pneumatic control devices typically deployed in glycol systems emit methane and VOCs. Chemical handling and maintenance requirements of glycol units in remote locations is also a challenging task. Glycol evaporation and condensation in downstream pipelines act as a source of corrosion and foaming problems in the downstream of amine plants. In contrast

to glycol and other dehydration methods, membrane technology has many advantages, such as small footprint area, easy operation without moving parts, no need for chemical reagents, lower energy requirements and also good reliability for operation in remote locations. Several research groups have shown a higher selectivity of water over methane using polymeric membranes [7,8]. Such technology is expected to reduce the dew point of the gas by 30-50 °C.

Many previously reported works have shown that incorporation of NPs into the polymeric matrix enhances the properties of polymers in various fields [9-13]. MMMs combine the advantages of excellent flexibility and ductility of the polymers [14] with functional properties of NPs, including chemical and optical properties [15,16], mechanical strength [14,17], high thermal stability [18] and high surface area to volume ratio [19,20]. Such characteristics suggest that these materials are able to improve the performance of industrial processes such as gas dehydration, textile and water absorption treatment.

To improve the gas dehydration process by the aid of MMMs, the performance of the selective and support layers of polymeric membranes should be enhanced. Many researchers have investigated the dehydration of methane gas and water vapor transport process through polymeric membranes [21-31]. In most of these works, the main problem in the process is the high resistance to water vapor transport of MPS layers in polymeric membranes. The support layers, which are usually fabricated by casting of polymer solutions, contribute to low porosity MPS films. Under these condi-

†To whom correspondence should be addressed.
E-mail: pdarvishi@yu.ac.ir

tions, the transport rate of water molecules through MPS layers is limited by the well-known concentration polarization phenomenon. At the best operating conditions, about 30% of the water vapor transmission resistance is due to selective layers, and 70% is due to support layers [30,31]. To overcome these problems, the physical structure of the support layers should be modified to provide supports with high porosity and flexibility. One efficient method for achieving enormous improvement in the polymer properties is the use of nanostructured polymers (NSPs). Among various techniques, nanoscale polymers and nanofibers are widely investigated to prepare NSPs. A number of methods have been used for synthesis of polymer nanofibers, among which electrospinning process seems to be the only reliable approach for massive production [32]. This method has been investigated and applied widely to many industrial applications such as ultrafiltration [33,34], clothing [35], air filtration [36,37] and energy recovery ventilators [38]. It is demonstrated that high water vapor permeation rates can be achieved by reducing the fiber diameters [36,37]. Based on the results obtained in our previous work [39], polyacrylonitrile (PAN) showed satisfactory performance in the water vapor transmission process, and it can be a reasonable choice for fabricating the ESNS.

Another significant issue in screening the polymeric membranes is the separation factor of selective layer. By applying a reliable technique of incorporation NPs into a hydrophilic polymer, the water vapor separation efficiency of selective layers may be improved. Among the hydrophilic rubbery polymers, Pebax 1657 is one of the favorite polymers in the process of water vapor separation. It is a commercially available polymer that contains a hydrophilic poly(ethylene oxide) (PEO) phase and a rigid glassy polyamide phase in its structure [40-42], which makes Pebax 1657 a reasonable polymer for the preparation of selective layers.

Among the various NPs, silica has unique properties that make them specific for water absorption and water vapor transmission processes. These properties include high surface area, inert nature, low toxicity, thermal stability, facile synthetic route, large-scale synthetic ability and the ability to be functionalized with a wide range of polymer molecules [13,43]. Silica NPs are highly hydrophilic materials in which the surface energy that is estimated from the specific interaction between the filler surface and polar chemicals is much higher for silica than other NPs such as carbon black [44]. Integration of these properties allows the nanocomposite polymers to have improved hydrophilicity, toughness, and permeability [45-48]. Another filler incorporated into Pebax 1657 is titanium dioxide, due to its hydrophilic nature and a wide range of applications [49-53].

In spite of the above considerations, the inclusion of NPs into the polymeric materials has some critical aspects. The dispersion of NPs should be uniform and avoid the NPs agglomeration tendency. In addition, a reasonable bonding between NPs and polymer matrix should be guaranteed [54]. In this case, the sol-gel process is effective and useful for the incorporation of NPs into the polymeric membranes. The operating temperature of this method is typically low, which minimizes the thermal volatilization and degradation of entrapped species. It also uses compounds that do not create impurities at the end of process, which makes it a waste-free technique with no need for a washing stage. Since NPs are synthesized in the polymer solution, the reticulation process may be disturbed and an optimal bond between inorganic and organic materials is expected [54,55]. The proper functionalization of NPs surfaces also improves the dispersion uniformity of NPs into the polymer matrix during the sol-gel process. By applying a suitable chemical group that assists regulating the properties of NPs for target characteristics, a reliable enhancement in NPs properties can be achieved. Glycols contain hydroxyl groups in their structure that gives them a wide variety of derivatives. These groups permit them to act as an intermediate in a wide range of reactions and processes, especially in water-related operations.

The existence of heavier hydrocarbons in the natural gas may also affect the dehydration process. Due to high condensability, heavier hydrocarbons can influence the permeance of methane and the nature of polymeric membranes. To the best of our knowledge, the work of Lin et al. [56] is the only published work that has been devoted to natural gas dehydration process to investigate the best design of this process and overcome the limitations of feed-to-permeate pressure ratio. Mixed-gas dehydration data are not widely available to see the effect of heavier hydrocarbons on natural gas dehydration process. Indeed, there are few works considering NPs as fillers in the polymeric membranes for water vapor separation [31,57,58]. Besides, there is no reported work to investigate the performance of sol-gel incorporation method into polymeric membranes with ESNS layers for dehydration of natural gas.

The present study is aimed to prepare MMMs with optimized properties in order to have a higher performance than the currently available material in the gas dehydration process. For this purpose, polymeric layers were prepared by electrospinning of PAN polymer to obtain support layers with high porosity and flexibility. After that, polymeric solutions of Pebax 1657 were prepared and the NPs were incorporated into the polymer matrix via sol-gel method. Then, the nanocomposite polymers were deposited on electrospun supports by dip-coating method. The fabricated membranes were tested for dehydration of methane and natural gas individually to show the effect of heavier hydrocarbon components on natural gas dehydration performance. The effect of process parameters such as feed and sweep gas flow rates, moisture content in the feed and feed pressure was also investigated. Finally, the mass transfer resistances of the support and selective layers were determined and analyzed in detail.

## MATERIALS AND METHODS

### 1. Chemicals

Polyacrylonitrile (PAN, average molecular weight=100,000) was provided by Esfahan Polyacryl Company, Iran. Pebax 1657 was purchased from Arkema, France. Tetraethyl orthosilicate (TEOS, purity=95 wt%) as silica precursor and N, N-dimethylformamide (DMF, purity=99 wt%) were supplied from Samchun, Korea. Hydrochloric acid (HCl, purity=37 wt%) and Ethylene glycol (EG, purity= 99.8 wt%) were purchased from Merck. Titanium isopropoxide (TTIP) as titania precursor was provided by Sigma Aldrich. Table 1 gives the characteristics of the materials used in this study. Nitrogen with a purity of 99.9% and methane with a purity of 99.95% were purchased from Farafan gas, Iran. Natural gas with the composition mentioned in Table 2 was supplied from national

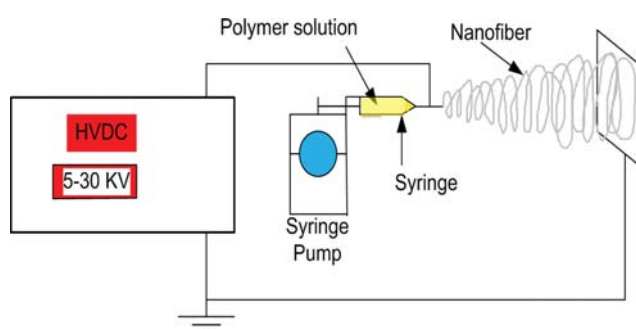**Table 1. Characteristics of chemicals used in the study**

| Material | CAS no. | MW | Density (g cm$^{-3}$) | Supplier |
|---|---|---|---|---|
| PAN | 25014-41-9 | 100000 | 1.184 | ESPC[*] |
| Pebax 1657 | Proprietary[**] | 60% PEO | 1.14 | Arkema |
| | | 40% PA6 | | |
| DMF | 68-12-2 | 73 | 0.93 | Samchun |
| Ethanol | 64-17-5 | 46.07 | 0.7893 | Samchun |
| TEOS | 78-10-4 | 208.33 | 0.933 | Samchun |
| HCL | 7647-01-0 | 36.5 | 1.18 | Merck |
| EG | 107-21-1 | 62.07 | 1.1132 | Merck |
| TTIP | 546-68-9 | 284.22 | 0.96 | Sigma Aldrich |

[*]Esfahan polyacryle company
[**]The specific chemical identity is withheld, as it is the confidential business information of Arkema Inc.

**Table 2. The composition of natural gas**

| Component | Methane | Ethane | Propan | Butane | Pentane | Hexane+ | $CO_2$ | $N_2$ |
|---|---|---|---|---|---|---|---|---|
| Mole percent | 88.01 | 4.02 | 1.13 | 0.39 | 0.11 | 0.06 | 0.07 | 6.21 |



**Fig. 1. A schematic diagram of the electrospinning setup.**

Iranian gas company (NIGC). All chemicals were used as received without further purification.

**2. Preparation of the Electrospun Support Layers**

Fig. 1 shows a schematic diagram of the electrospinning setup. The process involves the use of an electric field for fiber formation in which many parameters such as the distance between the syringe tip to the collector, solution concentration, solution viscosity, molecular weight of polymer, dielectric constant of the solvent, feeding rate, orifice diameter, the applied voltage, humidity and the surface tension of the polymer solution affect the formation of nanofibers [32]. The most effective parameter on fiber diameter is the polymer solution concentration [59-61]. Deitzel et al. [62] demonstrated that a higher fiber diameter will be obtained by increasing the polymer concentration according to the power law relationship. Demir et al. [63] showed that the fiber diameter is proportional to the cube of polymer concentration. Therefore, a minimum possible polymer concentration should be chosen to create ESNS layers with small fiber diameter and good morphology.

PAN solution was prepared by mixing 8 wt% of PAN powder with DMF and then stirring at 60 °C for 6 h until a well-dissolved solution with light yellow color was achieved. The stirring was continued at room temperature overnight. Once dissolved bubbles were

removed, the solution was placed in a 5 ml syringe with a spinneret at the head. The spinneret was installed 15 cm from a 10×20 cm flat-grounded copper collector. A 25 kV voltage was applied from a high voltage DC source that allowed the solution to jet from the syringe to the collector. The feed rate of solution was kept constant at 1.2 mL h$^{-1}$ using a controlled syringe pump. The electrospinning of PAN solution lasted for 4 h to achieve the appropriate thickness of support layer. To collect the nanofibers conveniently, a non-woven polyester support with high porosity (>60%) was used on the copper plate. This support helps to easily prepare smooth ESNS and increases the mechanical strength of the membranes.

**3. Fabrication of Mixed Matrix Membranes**

Pebax 1657 solutions were prepared by mixing 2 wt% of Pebax granules in a solvent composed of deionized water and ethanol (30 : 70 v/v), and then stirring for 12 h at 90 °C. Water is used as a co-solvent for the production of Pebax membranes and helps to separate the two phases of ethanol and Pebax polymer. It encourages the aggregation of polymers, simplifies the preparation of polymer solution and improves the performance of solvent. Without the use of water, droplets of ethanol coalesce into distinct domains and polymer is more randomly dispersed [64]. To prepare the nanocomposite solutions of the selective layers, the sol-gel methodology was utilized based on Stöber method [65]. Various amounts of TEOS were dissolved in the mixture of water/ethanol and stirred at room temperature for 30 min. Then, HCl was added dropwise to achieve a solution concentration of 0.1 M followed by stirring at 60 °C for 2 h. Finally, the Pebax 1657 solution was gradually added and the mixture was completely mixed at 60 °C for 60 min. In a similar way, TTIP was used instead of TEOS for preparation of MMMs containing titania NPs. Based on the hydrolysis reactions of the sol-gel process [66], each mole of TEOS produces one mole of silica and each mole of TTIP produces one mole of titania NPs. With this in mind, the required amounts of TEOS and TTIP are adjusted to prepare MMMs at the desired concentration of NPs. To functionalize the silica and titania NPs, EG was added to the

**Table 3. The concentration of NPs used in the fabricated membranes**

| Membrane | NPs | NP/Pebax 1657 (wt%) | EG/Pebax 1657 (wt%) |
|---|---|---|---|
| Pebax | - | - | - |
| Pebax-S5 | $SiO_2$ | 5 | - |
| Pebax-S15 | $SiO_2$ | 15 | - |
| Pebax-S30 | $SiO_2$ | 30 | - |
| Pebax-S50 | $SiO_2$ | 50 | - |
| Pebax-SE | $SiO_2$ | 30 | 15 |
| Pebax-T5 | $TiO_2$ | 5 | - |
| Pebax-T15 | $TiO_2$ | 15 | - |
| Pebax-T30 | $TiO_2$ | 30 | - |
| Pebax-T50 | $TiO_2$ | 50 | - |
| Pebax-TE | $TiO_2$ | 30 | 15 |

solutions after the addition of HCl, and then stirring was continued for 2 h at 60 °C. To complete the fabrication of nanocomposite membrane, the prepared solutions of Pebax 1657 with and without NPs were deposited on the ESNS of PAN via dip-coating method. Since the electrospun PAN supports are highly porous layers, some of the Pebax 1657 solution may penetrate through the support pores. To prevent forming a new layer in the membrane support, the penetrated solution was collected by a syringe from the bottom and around the membrane. The weight percent ratio of NPs and EG used in each membrane is summarized in Table 3.

**4. Membrane Characterization**

Field emission electron microscopy (HITACHI S 4160 FESEM, Japan) was used to examine the surface morphology of PAN nanofibers, and the NPs incorporated into the selective layers of Pebax 1657. X-ray diffractometer (Philips PW1830, Netherlands) was used to investigate the phase and crystalline state of MMMs. The surface chemistry of MMMs was examined by Fourier transform infrared

spectroscopy (ABB, BOMEM 102, Canada) in the range of 4,000-400 cm$^{-1}$.

**5. Permeation Measurement**

The MMMs were tested using a typical gas permeation setup (Fig. 2) for measuring the permeability of gases and water vapor. Pure methane or natural gas was introduced into the water bubbler at a controlled temperature to produce the wet gas. Then, the wet gas stream entered a demister to capture each droplet of liquid. The membrane permeation cell was fabricated from stainless steel and all sides of the membrane were sealed by O-rings. A rectangular porous plate made from stainless steel was used to withstand the feed side pressure. The plate was mounted in the cell to support the membrane sheet with an active area of 157 cm$^2$. Nitrogen was used as sweep gas in the permeate side of the membrane. The permeation cell was designed under sweep/countercurrent conditions to enhance the permeation of water vapor through the nanocomposite membrane. The water content in the feed, retentate and permeate streams was measured using a dew point sensor (S212, CSi-tec, Germany, measurement range: 0-100% RH) and the gas composition was analyzed by gas chromatography. The feed flow rate was measured using a mass flow meter (S420, CSi-tec, Germany, measurement range: 0-60 Nl/m).

Permeation tests were carried out for pure methane gas, pure nitrogen gas, methane/water and natural gas/water gas mixtures. The required time to reach steady state permeation data depends on the nature of gas and membranes. It was varied from 60 to 90 min. Each permeation test was carried out four times to decrease the uncertainty of experiments. Each measured data point in the current study is the average of four independent measurements. In addition, error bars are indicated for better comparison between different cases.

Heavier hydrocarbons (ethane, propane, and butane) and water vapor are highly condensable materials. Therefore, sorption of these components into MMMs may affect the nature of polymer matrix
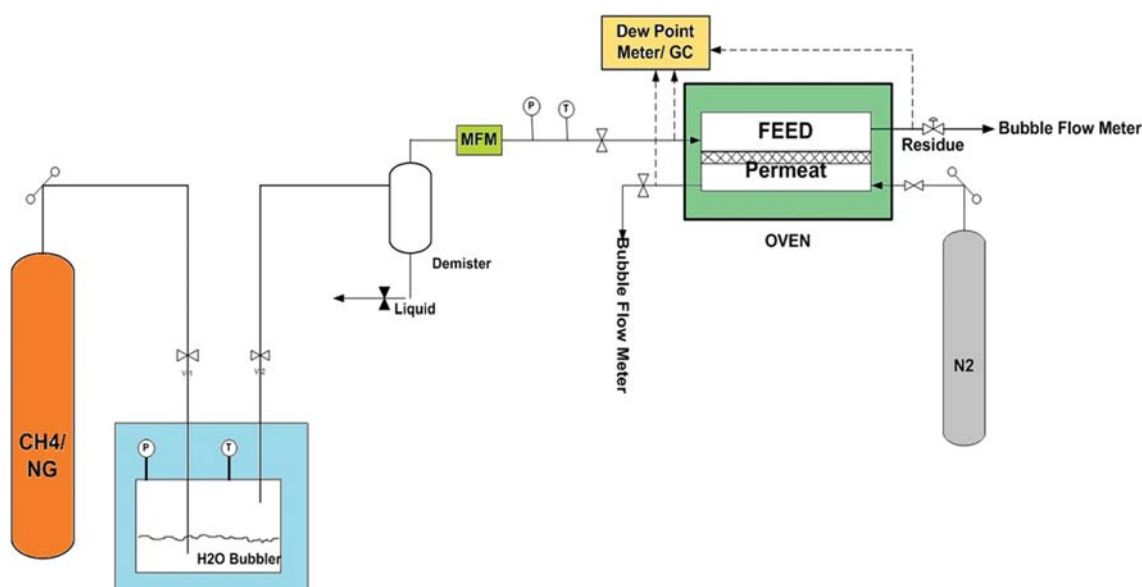


**Fig. 2. The schematic diagram of the sweep/countercurrent setup used to measure the permeance of water vapor and natural gas components through the mixed matrix membranes.**

and plasticize the polymer. To ensure that the fabricated membranes are not defected during dehydration tests, the permeance of nitrogen was measured before and after the natural gas dehydration tests. The highly condensable components evaporated after several hours of dehydration tests and their effect on the polymer chains disappeared. Thus, the nitrogen tests were carried out for each MMM right after the dehydration tests and continued for 24 h to obtain a constant $N_2$ permeation flux.

## 6. Determining the Properties of Mixed Matrix Membranes

6-1. Determination of Gas Permeance

The permeability of gas molecules within a polymeric film is defined as follows [67]:

$$P = \frac{Nl}{A(p_2 - p_1)} \tag{1}$$

Permeability coefficient is usually expressed in units of Barrers, where 1 Barrer $= 10^{-10}$ cm$^3$ (STP) cm/(cm$^2$ s cm Hg). To compare the performance of thin films with different thicknesses, permeance is used instead of permeability, which is defined as the permeability divided by the film thickness (P/$l$). The selectivity of a membrane for gas A relative to gas B is equal to the ratio of their permeances and is often expressed in gas permeation units (gpu), where 1 gpu $= 10^{-6}$ cm$^3$ (STP)/(cm$^2$ s cm Hg).

The selectivity of a membrane for gas A over gas B is the ratio of their permeances:

$$\alpha_{A/B} = \frac{\left(\frac{P}{l}\right)_A}{\left(\frac{P}{l}\right)_B} \tag{2}$$

Under mixed gas/water vapor conditions, the permeance of water vapor and other gases is determined from Eq. (3) and Eq. (4), respectively [30,56]:

$$\frac{P_w}{l} = \frac{N_w \cdot \ln\left(\frac{\Delta p_{w.L}}{\Delta p_{w.0}}\right)}{A(\Delta p_{w.L} - \Delta p_{w.0})} \tag{3}$$

$$\frac{P_g}{l} = \frac{N_g}{A\left(p_g^F - \frac{p_{g.0}^P}{2}\right)} \tag{4}$$

6-2. Determination of Fractional Free Volume

Based on the amounts of NPs and polymers used in the preparation of each MMM, the fractional free volume (FFV) of the membranes can be determined. FFV is an intrinsic property that affects the permeability and transport of gases through the membrane. It is created by the volume left between the entangled chains of polymer. The most common method to calculate this property for pure polymeric membranes (without NPs) is as follows [68]:

$$FFV = \frac{M_{Pebax/\rho_{pebax}} - 1.3V_{w, Pebax}}{M_{Pebax/\rho_{pebax}}} \tag{5}$$

where $M_{Pebax}$ is the molar weight of Pebax 1657 monomer (g/mol), $\rho_{Pebax}$ is the density of pure Pebax 1657 (g/cm$^3$) membrane, and $V_{W, Pebax}$ is the van der Waals volume of Pebax (cm$^3$/mol). The value of $V_W = 95.09$ cm$^3$/mol is obtained for Pebax 1657 based on Bondi's
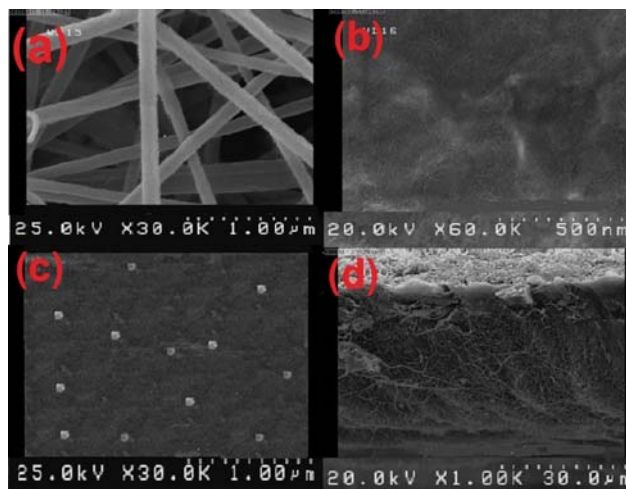


**Fig. 3. FESEM images of (a) electrospun support layer of PAN (b) the surface of composite pure Pebax membrane (c) the surface of Pebax-S15 mixed matrix membrane (d) the cross-sectional image of fabricated MMMs.**

group contribution method [69,70]. For the fabricated MMMs, the contribution of silica or titania NPs should be taken into account from the following equation [71]:

$$FFV = \frac{V_{MMMs} - \left[\left(\frac{1.3V_{w, Pebax}}{M_{Pebax}}\right)(1 - \varphi_{NPs}) + \left(\frac{\varphi_{NPs}}{\rho_{NPs}}\right)\right]}{V_{MMMs}} \tag{6}$$

where $V_{MMMs}$ is the specific volume of MMMs (cm$^3$/g) and $\varphi_{NPs}$ is the volume fraction of silica or titania NPs in the sample.

## RESULTS AND DISCUSSION

### 1. Membrane Characterization

Fig. 3 shows the FESEM images of the ESNS and selective layers. The image of PAN nanofibers is presented in Fig. 3(a) with a magnification of 30 kx and 1 μm scale. The nanofibers were fabricated by electrospinning method and used as support layers for membranes. The nanofibers exhibit a uniform and smooth surface, no beads, random orientation and a high porosity.

The nanofiber diameters were measured using the KLONK image software after the calibration of FESEM images based on their scale bars. The average fiber diameter based on measuring 100 different nanofiber diameters is 284±46 nm. This indicates that the fabricated ESNS have smaller fiber diameters than the electrospun membranes used for energy recovery ventilators [38]. Fig. 3(b) indicates the surface of composite membrane with no NPs with a magnification of 60 kx and 500 nm scale bar. Fig. 3(c) shows the surface of nanocomposite membrane containing 15 wt% of silica NPs (Pebax-S15) with a magnification of 30 kx and 1 μm scale bar. The FESEM images of other MMMs were similar to Fig. 3(c) with different concentrations of NPs. A representative cross-sectional image of the fabricated MMMs is shown in Fig. 3(d) with a magnification of 20 kx and 30 μm scale bar.

Fig. 4 illustrates the XRD patterns of silica NPs and the structural changes of MMMs due to the presence of silica NPs. Generally,
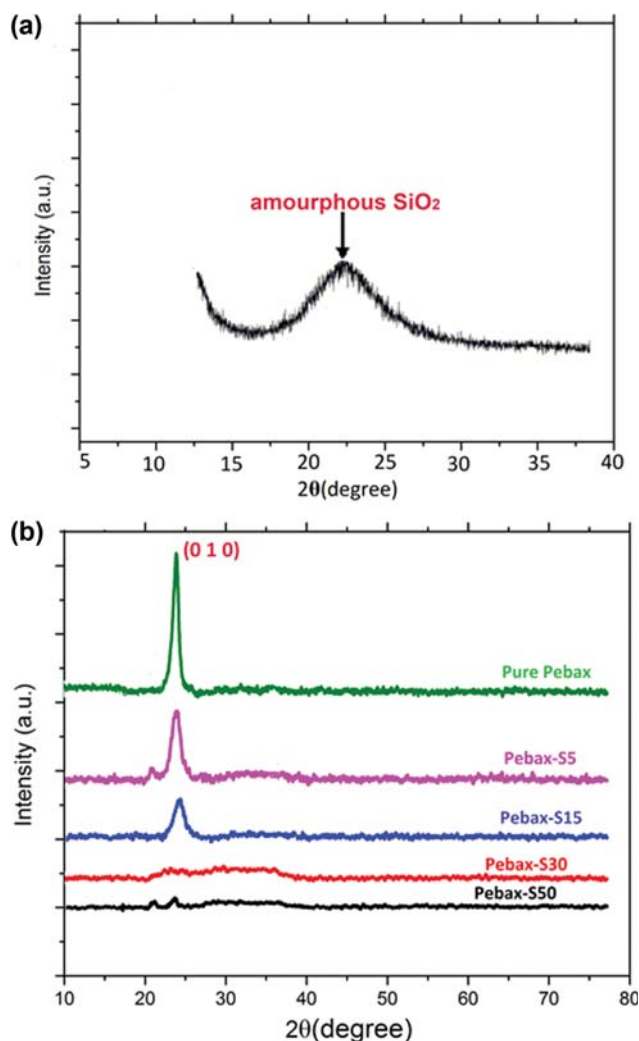
Fig. 4. XRD pattern of mixed matrix membranes for pure Pebax 1657, Pebax-S5, Pebax-S15, Pebax-S30, and Pebax-S50.

the sharp peaks with a strong intensity are related to the crystalline region, while broad peaks with a weak intensity are related to the amorphous state of materials [72,73]. The XRD spectrum of silica NPs is presented in Fig. 4(a). The figure indicates a broad and weak peak for the fabricated NPs via the sol-gel method, demonstrating that the synthesized silica NPs are amorphous materials. The absence of sharp peaks also confirms that the prepared silica NPs do not have crystalline structure.

The pure Pebax 1657 (Fig. 4(b)) has a sharp and strong peak at $2\theta=24.2^{\circ}$, resulting from polyamide 6 polymer via interchain hydrogen bonding. As illustrated in Fig. 4(b), the intensity of peak in MMMs of Pebax-S5, Pebax-S15, Pebax-S30, and Pebax-S50 decreases due to doping of silica NPs, implying that the amorphous region in the hybrid material is enhanced. Similar results were obtained for the MMMs containing $TiO_2$ NPs. As a result, increasing the titania concentration contributes to enlarging the amorphous region in the polymer matrix.

FTIR is a useful quantitative tool to identify chemical compounds and the functional groups in the polymeric samples and other products. Fig. 5 shows the FTIR spectra of pure Pebax 1657 and
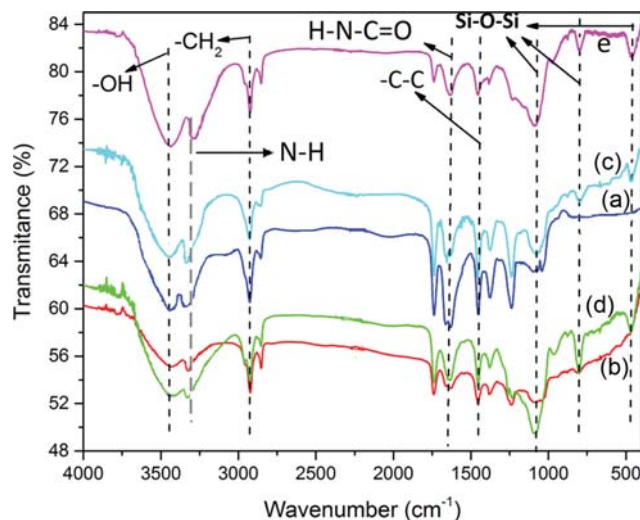


Fig. 5. FTIR spectra of mixed matrix membranes (a) Pure Pebax 1657 (b) Pebax-S5 (c) Pebax-S15 (d) Pebax-S30 (e) Pebax-S50.

the MMMs containing silica NPs in the range of 4,000 to 400 $cm^{-1}$. The bands at 3,290 and 1,641 $cm^{-1}$ are related to N-H and H-N-C=O groups, respectively. The peak at 2,940 $cm^{-1}$ is related to $-CH_2$ group and those in the range 1,452-1,500 $cm^{-1}$ are ascribed to C-C stretching vibrations. The band at 3,411 $cm^{-1}$ is ascribed to O-H group, which is presented during the hydrolysis step of the sol-gel method. The asymmetric and symmetric stretching of Si-O-Si as well as Si-O-Si bending are presented at 1,100 $cm^{-1}$, 800 $cm^{-1}$ and 470 $cm^{-1}$, respectively. The results of hybrid membranes containing titania NPs also indicate that titania NPs have optimal bonds with Pebax 1657 polymer. The presence of silica and titania NPs peaks on the FTIR of polymer suggests that the NPs are attached to polymers via chemical bands. This phenomenon was also reported previously for Polyurethane-silica [74] and Pebax-silica [73] hybrid membranes.

Good attachment and grafting treatment of NPs into the polymer matrix can deagglomerate the NPs [75]. Fig. 6 shows the FESEM images of various amounts of silica and titania NPs incorporated
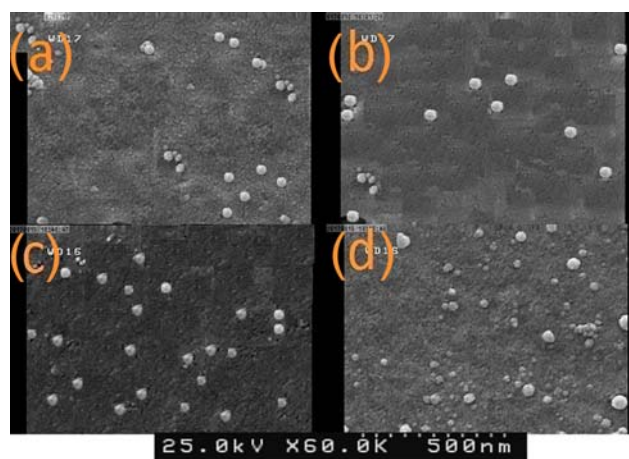


Fig. 6. FESEM images of the membranes surface for (a) Pebax-S5, (b) Pebax-T5, (c) Pebax-S15 and (d)Pebax-T15.

**Table 4. The transport properties of pure gases in mixed matrix membranes**

| Membrane | FFV | $N_2$ permeance (gpu) | $CH_4$ permeance (gpu) | Selectivity ($CH_4/N_2$) |
|---|---|---|---|---|
| Pebax | 0.102 | 0.83 | 1.1 | 1.32 |
| Pebax-S5 | 0.163 | 0.98 | 1.27 | 1.29 |
| Pebax-S15 | 0.236 | 1.09 | 1.39 | 1.18 |
| Pebax-S30 | 0.292 | 1.26 | 1.58 | 1.25 |
| Pebax-S50 | 0.447 | 2.26 | 3.23 | 1.43 |
| Pebax-SE | 0.342 | 1.71 | 1.72 | 1.0 |
| Pebax-T5 | 0.179 | 1.06 | 1.35 | 1.27 |
| Pebax-T15 | 0.248 | 1.17 | 1.44 | 1.23 |
| Pebax-T30 | 0.308 | 1.42 | 1.63 | 1.14 |
| Pebax-T50 | 0.461 | 2.48 | 3.46 | 1.39 |
| Pebax-TE | 0.354 | 1.87 | 1.84 | 1.01 |

into the Pebax 1657 polymer via sol-gel method. There is no evidence of NPs agglomeration in Pebax-S5, Pebax-T5, Pebax-S15, and Pebax-T15 membranes. The good distribution of silica and titania NPs into Pebax 1657 shows that the electrostatic forces between the NPs are weakened and the interactions with organic polymer are enhanced. The chemical bands between the NPs and Pebax 1657 polymer, and the proper distribution of NPs into the polymer matrix indicate that $SiO_2$ and $TiO_2$ NPs are grafted into the polymer matrix and the sol-gel reaction is carried out successfully.

**2. Permeation Properties of Nitrogen and Methane Pure Gases**

Table 4 indicates the FFV of MMMs fabricated in this study. As shown, there is an increasing trend for FFV of MMMs with enhancing the concentration of silica or titania NPs. The higher FFV of MMMs compared to pure Pebax 1657 results in an interstitial volume that is accessible to the polymer segments. This leads to higher chain mobility, higher gas permeability, and stronger interactions between fillers and polymers [76].

Table 4 also shows the pure gas permeance of fabricated membranes. The permeance of pure Pebax membrane for nitrogen is 0.83 and for methane is 1.1 gpu at 26 °C and 2.5 bar. These values are compatible with previous works [30,77] using Pebax 1657 for the selective layer of membrane, demonstrating that the fabricated membranes are defect free. The intrinsic permeability of Pebax 1657 films for nitrogen gas is 2.4 Barrer [77]. The actual thickness of the selective layers of MMMs was determined using the FESEM and KLONK image software. By measuring the thickness of selective layers at ten different locations randomly and averaging them, the actual thickness of the selective layer of MMMs was determined to be 3.12±0.23 μm.

In general, the permeance of MMMs for pure $N_2$ and $CH_4$ gases is higher than pure Pebax membrane. The permeances of Pebax-S50 and Pebax-T50 are more than twice the permeance of pure Pebax membrane. Functionalization of silica NPs also increased the permeance of $CH_4$ by 35.4% and that of $N_2$ by 12.4%. In the case of functionalized titania NPs, these results are 31.3% and 8.9% for $CH_4$ and $N_2$ permeance, respectively. In addition, the permeance of MMMs containing titania NPs for methane and nitrogen is more than the permeance of MMMs containing silica NPs,

which is due to the higher FFV of the MMMs containing titania NPs compared to silica NPs. The results for permeance of pure $N_2$ in MMMs of the present work are relatively in good agreement with the previous work containing silica NPs [73].

**3. The Permeance of Water/Methane Mixture**

Due to the high differences in critical temperature and molecular size of water and methane, it is expected that these molecules have different permeances. In this manner, a concentration gradient for the more permeable component (water) near the surface of membrane may be created [40,78]. The effect of this boundary layer is reduced by increasing the feed flow rate [40,78,79]. Therefore, it is necessary to measure the permeances of water and methane at different feed flow rates.

The permeance of water vapor at the feed flow rate of 0.2-8 normal liters per minute (Nlpm) is shown in Fig. 7. The feed gas was $CH_4$ containing 0.4 mol% water at 2.5 bar and 26 °C. The sweep gas was $N_2$ at 3 Nlpm and 30 kPa. The effect of feed boundary layer for each membrane is eliminated at a specified feed flow rate. Therefore, concentration polarization occurs in the feed side of membranes at low flow rates of the feed. These flow rates are higher for MMMs in comparison to pure Pebax membrane. The reason is the hydrophilic nature of silica and titania NPs, which absorb more water molecules and reduce the concentration of water on the feed side. The minimum required feed flow rate for each membrane to
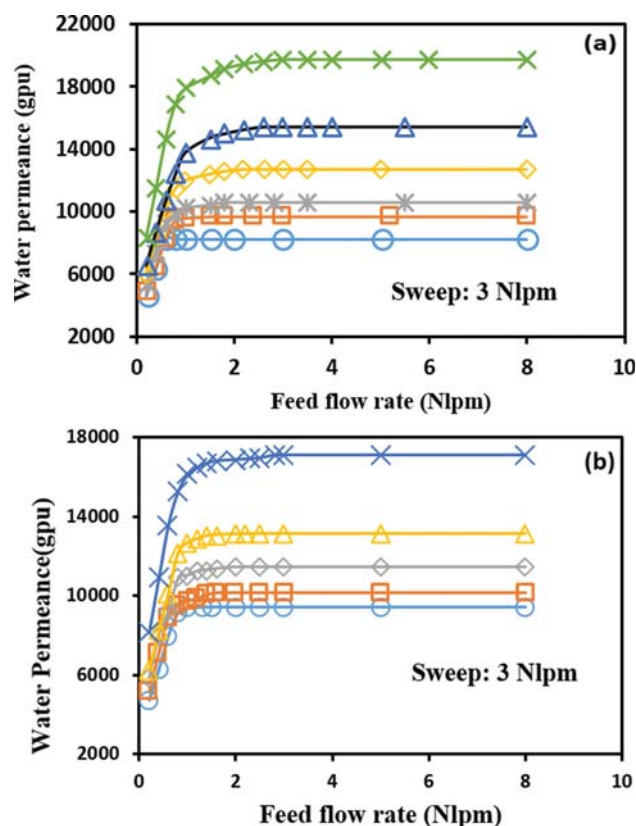


**Fig. 7. Water vapor permeance at different feed flow rates for (a) —○— Pebax —□— Pebax-S5 □ Pebax-S15 — Pebax- S30 —△— Pebax-SE × Pebax-S50 (b) —○— Pebax-T5 —□— Pebax-T15 —◇— Pebax-T30 —△— Pebax-TE × Pebax-T50.**

**Table 5. The minimum required feed flow rate to eliminate the boundary layer effect on the feed side**

|  | Pebax | Pebax-S5 | Pebax-S15 | Pebax-S30 | Pebax-SE | Pebax-S50 |
|---|---|---|---|---|---|---|
| Minimum flow rate (NLPM) | 0.6 | 1.5 | 1.8 | 2.2 | 2.6 | 3 |
|  | Pebax-T5 | Pebax-T15 | Pebax-T30 | Pebax-TE | Pebax-T50 | |
| Minimum flow rate (NLPM) | 1.3 | 1.6 | 2 | 2.2 | 2.8 | |

eliminate the effect of the boundary layer in the feed side is given in Table 5.

The equilibrium permeance of water vapor through pure Pebax is about four-times the permeance of membranes that used MPS in their structure [30]. The water vapor permeance of MMMs containing more than 15 wt% of NPs is more than 10,000 gpu, which is a criterion for commercially available materials [38]. The enhancement of water vapor permeance compared to previous MPS and ESNS membranes is due to both incorporations of NPs in the selective layer and the smaller fiber diameters of ESNS. The permeance of $CH_4$ was also measured at the same conditions of feed and the results are presented in Fig. 8. By changing the feed flow rate, the permeance of methane remains constant. The feed composition mainly consists of methane and there is no concentration gradient for this component in the feed side. These results are consistent with the data obtained in the previous work for pure Pebax membrane [30].

**4. Effect of Sweep Gas Flow Rate**

Fig. 9 shows the effect of sweep gas flow rate on the permeance of water vapor. The feed flow rate is 3.5 Nlpm at the conditions of 2.5 bar, 26 °C and 0.4 mol% of water vapor. The effect of sweep gas flow rate on permeance of methane gas is negligible and the $CH_4$ permeance is the same as shown in Fig. 8. As a result, the support layers of membranes show no resistance to methane permeance, and there is no boundary layer effect at the permeate side of membrane. However, the change of water permeance with increasing the sweep flow rate shows that even electrospun support layers exert some resistance to water vapor transmission. On the other hand, the water vapor permeance is enhanced by increasing the sweep gas flow rate. Sweep gas removes the water molecules that diffuse to the permeate side and increases the water partial pres-
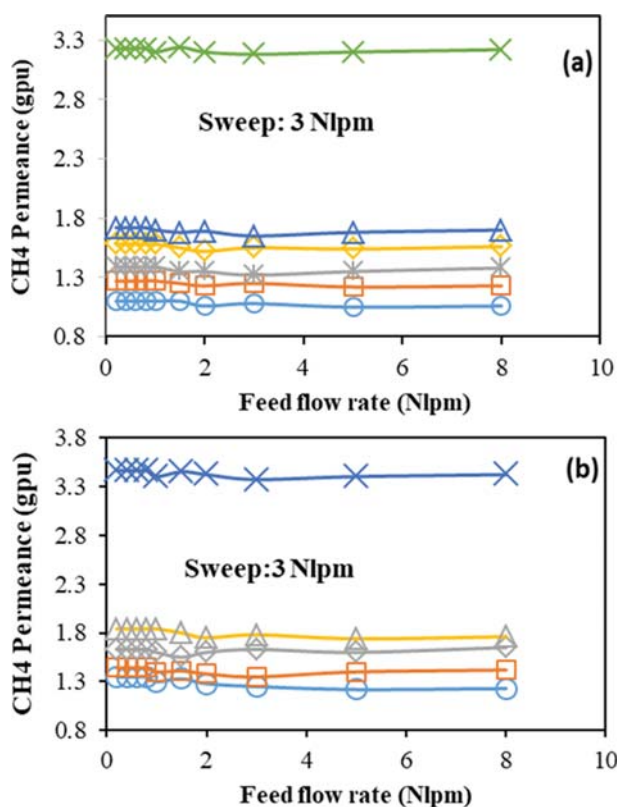


Fig. 8. Permeance of $CH_4$ at different feed flow rates (a) —○— Pebax —□— Pebax-S5 ✳ Pebax-S15 —◇— Pebax-S30 —△— Pebax-SE ✕ Pebax-S50 (b) —○— Pebax-T5 —□— Pebax-T15 —◇— Pebax-T30 —△— Pebax-TE ✕ Pebax-T50.
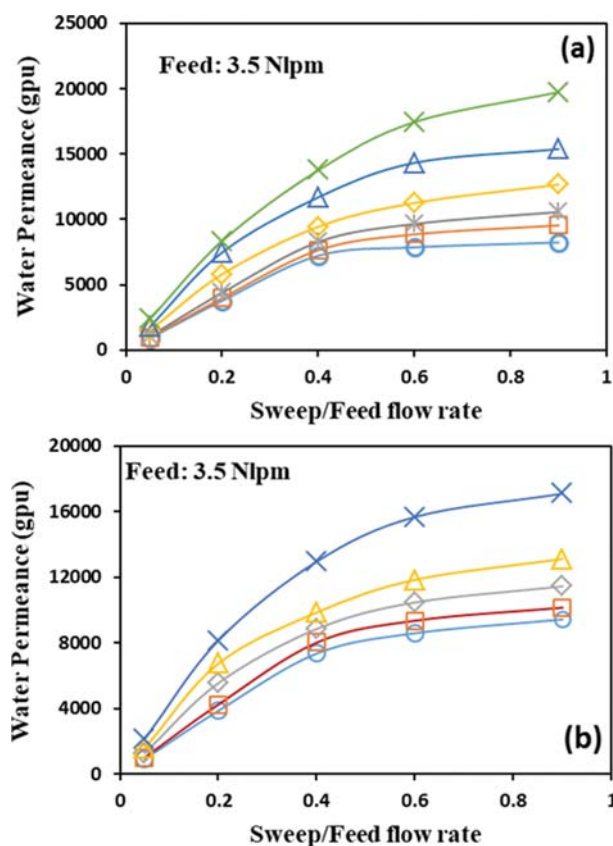
Fig. 9. Effect of sweep gas flow rate on water vapor permeance for (a) —○— Pebax —□— Pebax-S5 ✳ Pebax-S15 —◇— Pebax-S30 —△— Pebax-SE ✕ Pebax-S50 (b) —○— Pebax-T5 —□— Pebax-T15 —◇— Pebax-T30 —△— Pebax-TE ✕ Pebax-T50.
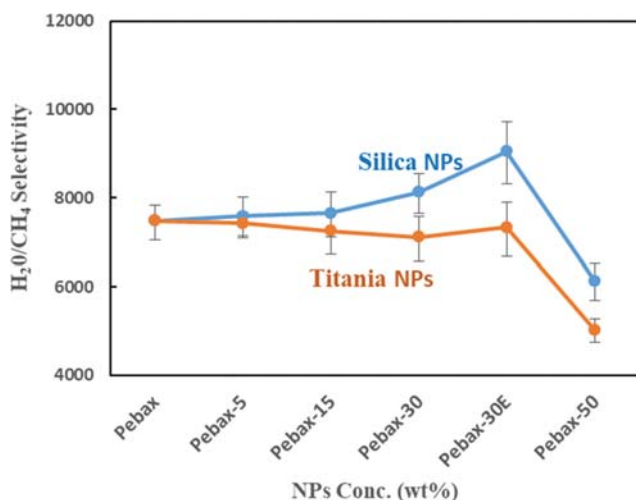
Fig. 10. H$_2$O/CH$_4$ selectivity of the mixed matrix membranes.

sure across the membrane.

5. H$_2$O/CH$_4$ Selectivity

The separation of water vapor from methane is very important in the dehydration process of natural gas. Therefore, the selectivity of fabricated MMMs is the dominant factor in the separation process. The selectivity of membranes versus the concentration of NPs is shown in Fig. 10. The addition of NPs to Pebax polymer enhances the permeance of both water vapor and methane gas. Incorporation of silica NPs up to 30 wt% increases the selectivity of water over methane gas. Functionalization of silica NPs by EG also increases the selectivity by 13.3%. At higher concentrations of silica NPs, the increase in methane permeance is more than water, and so the selectivity of MMMs is decreased.

As given in Table 4, the permeance of pure CH$_4$ in the MMMs containing titania NPs was more than MMMs containing silica NPs, due to higher FFVs. Thus, the selectivity of MMMs containing titania is less than those containing silica, and even is less than pure Pebax polymer. This indicates that there is a strong tendency for the formation of cavities on the polymer-titania NPs interface. Based on these findings, it is concluded that silica NPs compared to titania NPs have better compatibility with Pebax 1657 copolymer, and they can be suggested for fabricating the MMMs that enhance the gas dehydration performance. As a result, pure Pebax and the MMMs containing silica NPs were selected to investigate the effects of other parameters on the performance of fabricated membranes.

6. Effect of Feed Moisture Content

The effect of water vapor activity on water vapor permeance in Pebax membranes is shown in Fig. 11. The feed flow rate was 3.5 Nlpm at 2.5 bar and 26 °C and the sweep flow rate iwass 3 Nlpm at 30 kPa and 24 °C. The results indicate that the water vapor activity of the feed has a little effect on water vapor permeance of pure Pebax membrane, which is consistent with previously reported works [30]. The presence of silica NPs in the polymer matrix enhances the water vapor permeance. Silica NPs are hydrophilic inorganic materials that absorb water molecules and cause transmission of more water vapor. This effect is enhanced by doping the silica NPs
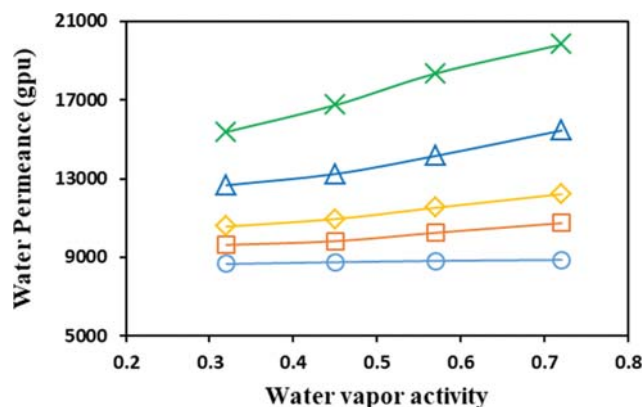


Fig. 11. Effect of moisture content on water vapor permeance of —○— Pebax —□— Pebax-S5 —◇— Pebax-S15 —△— Pebax-S30 ✕ Pebax-SE.

in MMMs. The Pebax-S30 membrane has a 20% higher water vapor permeance at the water vapor activity of 0.7 than that of 0.2. Functionalization of silica NPs by EG also enhances the water vapor permeance more than 20% compared to MMMs without EG. Glycols contain hydroxyl groups in their structure, which helps absorption of water molecules via hydrogen bonds.

7. Effect of Feed Pressure on Water and Methane Permeances

In the industry, the gas dehydration process operates at higher pressures than bench scale. The effect of feed pressure on the per-
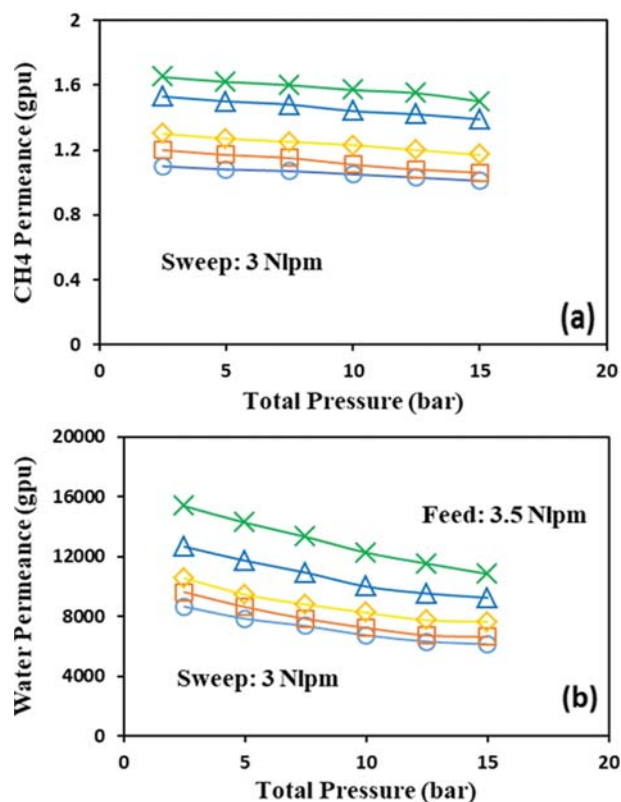


Fig. 12. Effect of feed total pressure on (a) methane and (b) water vapor permeance —○— Pebax —□— Pebax-S5 —◇— Pebax-S15 —△— Pebax-S30 ✕ Pebax-SE.

meation of water vapor and methane gas is investigated in Fig. 12. The feed with 0.4 mol% of water vapor had a flow rate of 3.5 Nlpm at 26 °C and the sweep flow rate was 3 Nlpm at 30 kPa and 24 °C. The results indicate that the permeance of $H_2O$ and $CH_4$ is decreased by increasing the feed pressure. The permeance is reduced 8.2% for methane and 29% for water vapor at the feed pressure of 15 bar. The reduction in the permeance of $CH_4$ gas can be explained by the polymer compression, which reduces the free volume of polymer matrix [80]. The reduction in water vapor permeance is more than methane and is related to the decrease of water vapor diffusion coefficient in the feed side. The mass transfer coefficient in the feed side depends on the hydrodynamics and geometry of the system, which is usually expressed in terms of Sherwood number [81]:

$$Sh = a \ Re^b Sc^c \left(\frac{L}{d_h}\right)^d = \left(\frac{kd_h}{D}\right) \tag{7}$$

where $Re = \left(\frac{\rho v d_h}{\eta}\right)$, $Sc = \left(\frac{\eta}{\rho D}\right)$, and a, b, c, and d are empirical constants dependent on the geometry of the system. The diffusion coefficient of water vapor in gases such as nitrogen and methane is proportional to the inverse of pressure, as introduced by Massman [82]:

$$D = D_0 \left(\frac{p_0}{p}\right) \left(\frac{T}{T_0}\right)^{1.81} \tag{8}$$

In the feed gas containing a mixture of water and methane, the fast transmission rate of water molecules is limited by its transport from the gas bulk to the surface of membrane. At two different feed pressures, the following relation is obtained from Eq. (7):

$$\frac{k_1 D_2}{k_2 D_1} = \left(\frac{\rho_1 v_1 \eta_2}{\rho_2 v_2 \eta_1}\right)^b \left(\frac{\eta_1 \rho_2 D_2}{\eta_2 \rho_1 D_1}\right)^c \tag{9}$$

If the increase in viscosity with pressure is negligible and the tests are carried out at the same feed flow rate, Eq. (9) is simplified as follows:

$$\frac{k_1}{k_2} \propto \rho^{b+1/c} D^{1+1/c} \tag{10}$$

As the feed pressure increases, gas density increases in contrast to diffusion coefficient. Most of empirical relations considered a value of 0.33 for c, and b is varied from 0.46 to 0.91 [81]. As a result, the diffusion term prevails in Eq. (10), which reduces the mass transfer rate, and consequently the water vapor permeance at higher pressures.

Metz et al. [40] reported 50% reduction in water vapor permeance by increasing the feed pressure from 2 to 15 bar, but they decreased the feed flow rate by increasing the feed pressure. George et al. [83] changed the feed pressure from 2 to 7.5 bar and reported almost the same values of water vapor permeability. However, by increasing the feed pressure, they increased the feed flow rate. Therefore, it can be concluded from the results of this study and the comparison with previous works that increasing the feed flow rate can reduce the effect of pressure increasing. By increasing the feed flow rate, the velocity of gas in the feed side increases. This promotes the mixing phenomenon and reduces the concentration polarization
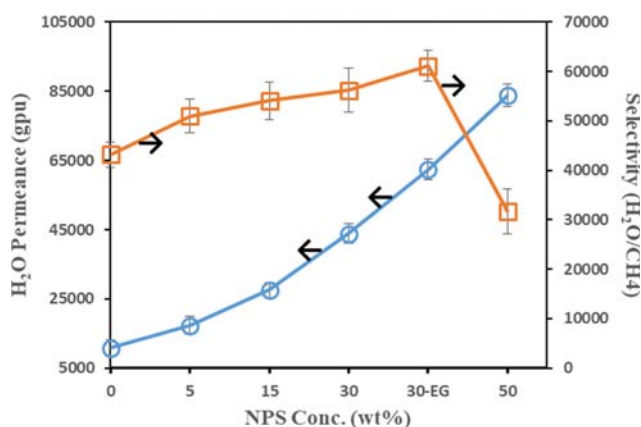


Fig. 13. Water vapor permeance and the $H_2O/CH_4$ selectivity in the tests of natural gas dehydration.

on the feed side.

**8. Effect of Heavier Components in Natural Gas Dehydration**

The water vapor permeance and its selectivity over methane are shown in Fig. 13. The tests of natural gas dehydration were carried out at a feed flow rate of 3.5 Nlpm under the conditions of 2.5 bar, 26 °C and the sweep gas flow rate of 3 Nlpm at 30 kPa and 24 °C. Enhancement in the permeance of water is due to the presence of heavier hydrocarbons and NPs, which increases the membrane free volume. In high concentrations of silica NPs (e.g., 50 wt% for the mixture of water/methane), the selectivity reduces
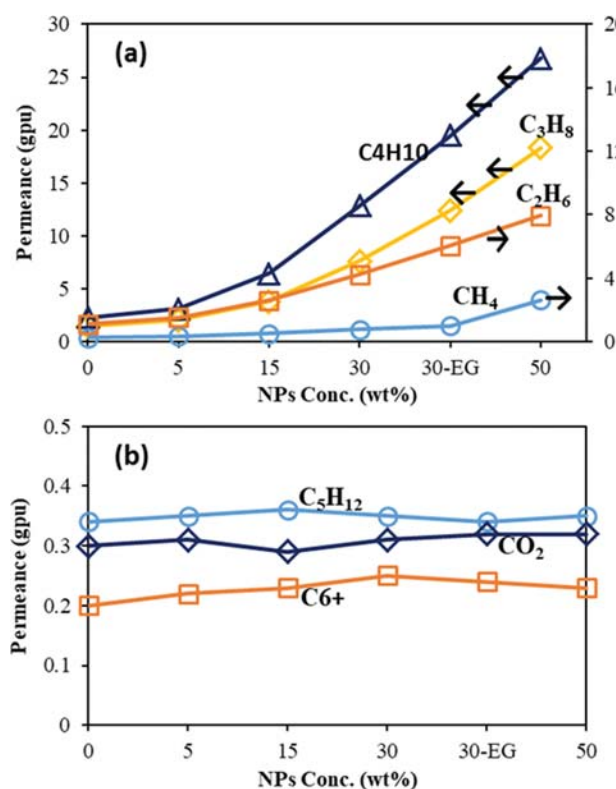


Fig. 14. (a) Permeance of methane, ethane, propane and butane (b) permeance of pentane, Hexane+ and $CO_2$ in the tests of natural gas dehydration.

**Table 6. Economic values for the main components of natural gas**

| Component | Criteria | Value |
|---|---|---|
| $CH_4$ | 9 cent per cubic meter | (about 139 $ per ton) |
| $C_2H_6$ | $ per ton | 240 |
| C3H8 | 105.85+6.65×oil price | about 438 $ per ton |
| C4H10 | 105.85+6.65×oil price | about 438 $ per ton |

because of more increase in the polymer free volume.

The permeance of methane and other components is shown in Fig. 14. Since the solubility selectivity is a dominant mechanism in rubbery polymers [74], the permeance of components is improved by increasing the permeate condensability. Condensability is often linked to the size of molecules, and heavier hydrocarbons permeate more than the lighter ones. Hence, heavier hydrocarbons make trouble for methane permeation and cause depletion in methane permeance. In other words, heavier hydrocarbons obstruct the methane permeation path in the matrix of membrane. This can be defined as the methane blocking ratio (MBR), which is the ratio of methane gas that does not permeate through the membrane due to the presence of heavier hydrocarbons [84].

As indicated in Fig. 14(b), the permeance of pentane, hexane+ and $CO_2$ is low and nearly constant in the natural gas dehydration tests. Two reasons may describe this behavior. First, the amount of $CO_2$ in the natural gas composition is very low (Table 2), which allows it to permeate completely in all fabricated MMMs. The second reason is the presence of other components in the natural gas that compete with $CO_2$. Although by increasing the concentration of NPs, the FFV of MMMs is enhanced, the other components with high concentration in the mixture compete with $CO_2$ and don't allow it to permeate faster. As a result, incorporation of NPs into the membranes has very little effect on the permeation of $CO_2$ and other components of natural gas with negligible concentration.

More permeation of heavier hydrocarbons and methane blocking in the fabricated membranes results in a high water-vapor permeation and selectivity in the natural gas dehydration process (Fig. 13). Although the permeance of $CH_4$ reduces significantly, the other valuable components of natural gas are lost during their permeation through membranes. In this case, the obtained selectivity of water over methane may not be practicable from the economical point of view. The value of the main components of natural gas in national Iranian oil company (NIOC) is given in Table 6. Since heavier hydrocarbons are more valuable than methane, the economic selectivity for the gas dehydration process is defined as follows:

$$\alpha = \frac{\left(\frac{P}{l}\right)H_2O}{\sum_{n=1}^{n=4}\left(\frac{P}{L}\right)CnH_{2n+2}} \tag{11}$$

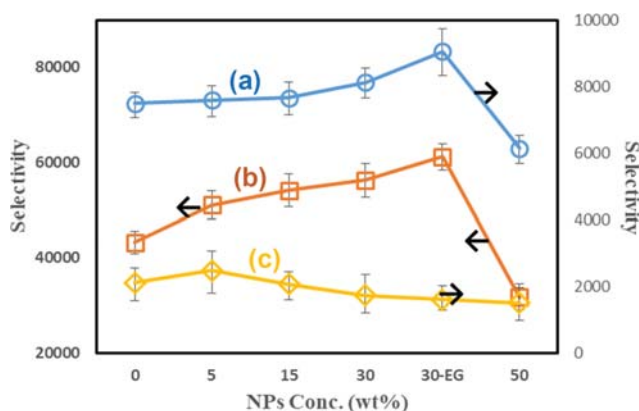Based on this definition, the selectivity of water vapor is calcu-



**Fig. 15. (a) Selectivity of $H_2O/CH_4$ when the feed consists of methane and water only (b) selectivity of $H_2O/CH_4$ when the feed contains water/natural gas (c) economic selectivity.**

lated with respect to all valuable components that permeate through the membrane. The permeation of pentane, hexane+ and $CO_2$ are not considered in Eq. (11) due to their negligible concentration in the natural gas. In Fig. 15, the calculated selectivities are compared with the corresponding values obtained for $H_2O/CH_4$ in the mixture of water/methane and water/natural gas. The economic selectivity was 2109 for pure Pebax membrane, increased to 2475 for Pebax-S5 MMM and then decreased slightly. This reduction is due to the higher permeability of heavier hydrocarbons than methane. Therefore, the optimum concentration of silica NPs for dehydration of natural gas is 5 wt%.

**9. Changing of Membrane Nature**

In the case of polymer softening, the permeation of an inert gas such as nitrogen with no effect on polymer chain will vary greatly [74]. Therefore, to ensure the accuracy of the obtained selectivities, it is necessary to measure the permeance of nitrogen after the dehydration of methane and natural gas tests. The experiments were performed at 2.5 bar and 26 °C, and the results are compared in Table 7. The non-change in nitrogen permeability indicates no evidence of plasticization in electrospun MMMs fabricated by the sol-gel method from Pebax 1657 and silica NPs.

Another aspect that should be clarified for the MMMs of Pebax 1657 is the permanent contact of copolymer with water molecules. Although water is used as a co-solvent for preparation of Pebax 1657 membranes, the solubility of water in Pebax is low. This is due to the hard segment of polyamide in the structure of Pebax 1657 copolymer, which does not swell readily in water [25]. Pebax 1657 is also insoluble in water. Different grades of Pebax were tested in boiling water for 7 days, and the results showed a negligible effect on the polymer structure [85].

**10. Membrane Resistance to Water Vapor Transmission**

In the previous sections, it was indicated that the sweep gas flow

**Table 7. Permeance of nitrogen before and after the natural gas dehydration tests**

| $N_2$ permeance (gpu) | Pebax | Pebax-S5 | Pebax-S15 | Pebax-S30 | Pebax-SE | Pebax-S50 |
|---|---|---|---|---|---|---|
| Before | 0.83 | 0.98 | 1.09 | 1.26 | 1.71 | 2.26 |
| After | 0.84 | 0.98 | 1.12 | 1.25 | 1.75 | 2.32 |

rate has no effect on the permeation of methane gas. The transport resistance to methane gas lies only in the selective layers and no resistance is applied by ESNS. In contrast, the permeance of water vapor increased by increasing the flow rate of sweep gas. As a result, there are some applying resistances to water vapor transmission by ESNS that should be determined. Based on existing empirical relations, the overall resistance to mass transfer is described by adding all layer resistances in series and the inverse of the permeance is considered as the transport resistance [78,86-88]. For pure Pebax and MMMs, the following relation can be used for estimating the transport resistance:

$$\frac{1}{k} = \left(\frac{l}{P}\right)_{sl} + \frac{1}{a\,v_s^b} \tag{12}$$

where $1/k$ is the overall resistance, which is equal to the inverse of membrane permeance, $(l/P)_{sl}$ is the resistance relevant to the selective layer of membrane and $1/a\,v_s^b$ is the resistance of support layers, which is empirically related to the sweep gas flow rate. $1/k$ is plotted as a function of $v_s^b$ and the value of b should be chosen to obtain the best fit. Fig. 16 shows the fitting of data for Pure Pebax and MMMs containing silica NPs. The parameters of Eq. (12) are

Table 8. Parameters of Eq. (12) for each membrane

| Membrane | a (gpu Nlpm$^{-b}$) | B | R$^2$ | Selective layer permeance (gpu) |
|---|---|---|---|---|
| Pebax | 7759 | 1.2 | 0.9991 | 14017 |
| Pebax-S5 | 8322 | 1.2 | 0.9995 | 15581 |
| Pebax-S15 | 9038 | 1.2 | 0.9996 | 17271 |
| Pebax-S30 | 13137 | 1.2 | 1 | 17500 |
| Pebax-SE | 18740 | 1.3 | 0.9999 | 19716 |
| Pebax-S50 | 17391 | 1.1 | 0.9999 | 29850 |

determined (Table 8) to demonstrate the contribution of each layer to the total resistance of water vapor transmission.

Fig. 17 shows the total resistance and the resistances relevant to ESNS at 3 Nlpm of sweep gas. It can be seen that by increasing the concentration of silica NPs, the total resistance of MMMs is decreased. This alleviation is 58.3% for Pebax-S50 compared to Pebax without NPs, which is due to the hydrophilic nature of silica NPs and the higher FFV of MMMs. Increasing the NPs concentration reduces the support resistance less than the total resistance, because
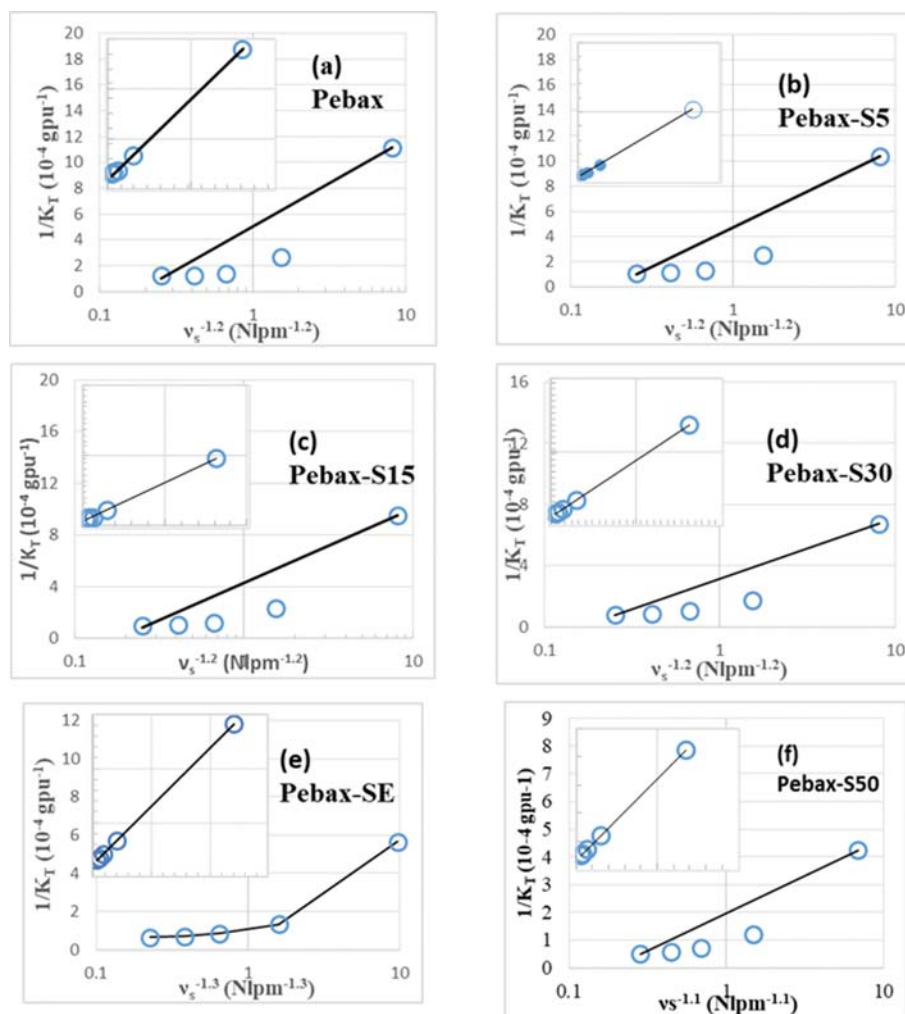


Fig. 16. Correlation of water vapor resistances and sweep flow rate of the membranes.
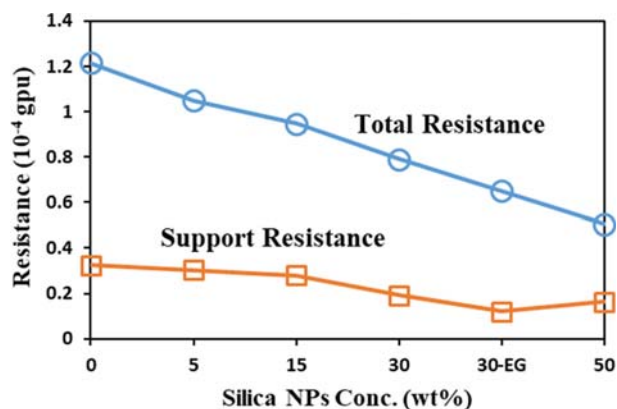
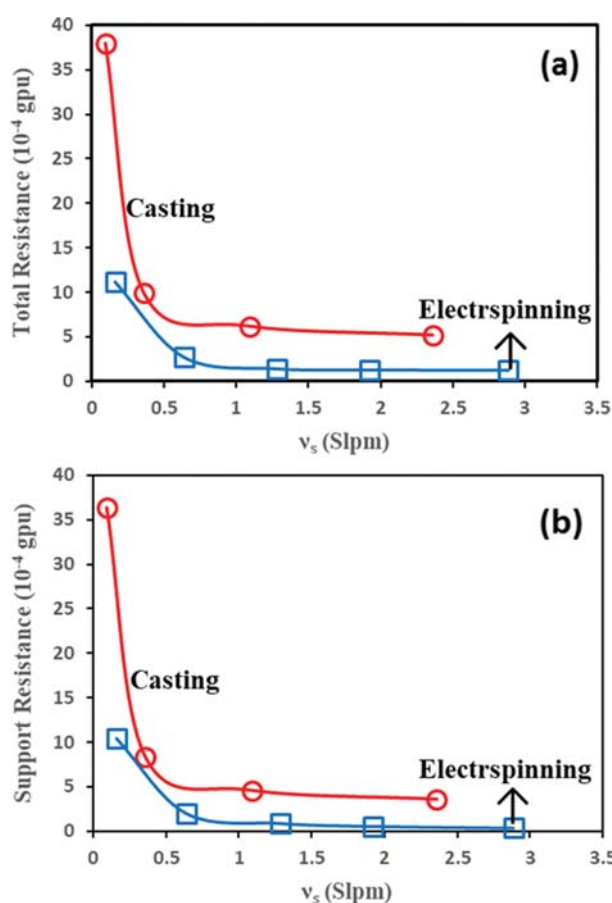Fig. 17. Total and support resistances of the membranes.



Fig. 18. Comparing the results of this work with the work of Hai-qing Lin et al. [30] (a) total (b) support resistances.

the NPs are incorporated into the selective layer of membranes.

In Fig. 18, the total and support resistances of the ESNS prepared in this work are compared with MPS membranes reported by Haiqing Lin et al. [30] for pure Pebax 1657 at various flow rates of sweep gas. The results indicate that electrospinning methodology is able to reduce the total water vapor transport resistances of polymeric membranes by 75.2%. In addition, the contribution of support layers at the best operating conditions (the highest sweep

gas flow rate) is alleviated from 67% in MPS membranes [30] to less than 30% in ESNS ones.

Based on the high reduction in total resistance of the prepared membranes in this study compared to MPS membranes, it can be concluded that for the same feed flow conditions, the ESNS membranes require much less membrane area. The cost of membrane module in this study is estimated to be \$103/m$^2$ based on the materials used and the cost of fabricating membrane sheet and module. This value is \$110/m$^2$ for MPS membranes [89]. There is not much difference in the preparation of one square meter of ESNS and MPS membranes due to almost the same amounts of chemicals consumed. However, for the same conditions of feed flow rate, the required membrane area is reduced to 40% when the membranes prepared in this study are used instead of MPS membranes. As a result, the cost of the membrane module fabricated in this study can be estimated to be 40% of MPS.

In the economic assessment of membrane-based gas dehydration system, the total separation cost (TSC) is usually considered. Basafaa and Pourafshari Chenar [89] reported the TSC of 0.2 \$/MSCM of feed for MPS membranes when the $H_2O/CH_4$ selectivity is about 500 and the permeance of $H_2O$ is 1,000 gpu at feed flow rate of 2.84 MMSCMD, feed pressure of 5,500 kPa, and inlet temperature of 30 °C. As shown, the economical selectivity of fabricated MMMs was more than 2000 and the permeance of water vapor was more than 6,000 gpu in the natural gas dehydration test. Consequently, the TSC for the prepared membranes is estimated to be less than \$0.05/MSCM.

## CONCLUSION

By introducing more efficient and chemically durable MMMs, it can be expected that polymeric membranes will play an increasing role in natural gas processing systems. Applying both electrospinning and sol-gel incorporation techniques in the fabrication of polymeric membranes can improve the performance of the water vapor transport process. In the present study, the electrospinning technique with the aid of sol-gel method was utilized to enhance the performance of composite polymeric membranes in the gas dehydration process. The resistance of composite membranes to water vapor transmission was reduced by 75.2% using the electrospinning methodology. In addition, the permeance of mixed matrix membranes was enhanced by applying the sol-gel method for incorporating the NPs into the polymeric matrix. These permeances are higher than commercially available materials and can be definitely introduced to the industry. It was also shown that the loss of heavier hydrocarbons in the natural gas dehydration process is a significant aspect, which should be considered in the design of required materials. A countercurrent design using a dry sweep gas stream and the use of permeate stream as fuel is suggested to be investigated in a semi-industrial pilot plant. In the future work, hollow nanofiber polymers will be considered for the natural gas dehydration process that is expected to have much more reduced resistances than this study. These kinds of materials are usually produced by two different methods, including the chemical vapor deposition (CVD) method [90] and direct co-axial spinning method [90,91]. To produce hollow nanofibers by the CVD method, the first pre-

cursor polymer is transformed to a nanofiber or "template" by a conventional electrospinning method. Then, they are coated with proper polymers or metals. Finally, hollow fibers are fabricated by dissolving the template material and drying them with centrifugal rotation dryers or by calcining in furnaces. The co-axial spinning is more regarded by researchers for fabricating hollow nanofibers. A jet is formed by a coaxial spinneret when two different polymer solutions flow through outer and inner capillaries simultaneously and the core material is dissolved with a selective solvent at the end of the process.

## ACKNOWLEDGEMENT

## NOMENCLATURE

P : permeability [Barrer]
N : flux [$cm^3\ s^{-1}$]
l : membrane thickness [cm]
A : membrane surface area [$cm^2$]
$P_1$ : downstream pressure [cmHg]
$P_2$ : upstream pressure [cmHg]
$\Delta p_{w,L}$ : pressure difference of water at the exit of the feed [cmHg]
$\Delta p_{w,0}$ : pressure difference of water at the entrance of the feed [cmHg]
$p_g^F$ : partial pressure of the gas at the feed side [cmHg]
$p_{g0}^P$ : partial pressure of the gas at the permeate side [cmHg]
$\alpha$ : selectivity
Sh : Sherwood number
Re : Reynolds number
Sc : Schmitt number
k : mass transfer coefficient [m/s]
$d_h$ : hydraulic diameter [m]
$\rho$ : density [$kg/m^3$]
$\eta$ : viscosity [Pa·S]
D : water diffusion coefficient [$m^2$/s]
$v_s$ : sweep gas flow rate [Nlpm]
Nlpm : normal liter per minute

### Abbreviations

NPs : nanoparticles
PAN : polyacrylonitrile
MMM : mixed matrix membrane
ESNS : electrospun nanofibrous support
MPS : microporous support
EG : ethylene glycol
NSPs : nanostructured polymers
VOC : volatile organic compounds
TTIP : titanium isopropoxide
TEOS : tetraethyl orthosilicate
DMF : dimethyleformamid
WVTR : water vapor transition rate
NIOC : national iranian oil company
NIGC : national iranian gas company

## REFERENCES

1. A. Sakheta and U. Zahid, *Chem. Eng. Res. Des.*, **137**, 70 (2018).
2. Z. Y. Kong, A. Mahmoud, S. Liu and J. Sunarso, *J. Nat. Gas Sci. Eng.*, **56**, 486 (2018).
3. M. Neagu and D. L. Cursaru, *J. Nat. Gas Sci. Eng.*, **37**, 327 (2017).
4. M. G. R.S. Santos, L. M. S. Correia, J. L. de Medeiros and O. D. F. Araujo, *Cheric*, **149**, 760 (2017).
5. S. H. Rajaee Shooshtari and A. Shahsavand, *Appl. Therm. Eng.*, **139**, 76 (2018).
6. K. Dalane, H. F. Svendsen, M. Hillestad and L. Deng, *J. Membr. Sci.*, **556**, 263 (2018).
7. C. A. Scholes, G. W. Stevens and S. E. Kentish, *Fuel*, **96**, 15 (2012).
8. R. W. Baker, Vapor and Gas Separation by Membranes, in: Adv. Membr. Technol. Appl., Wiley, New York (2008).
9. B. T. V. Sreekumar, T. Liu, B. G. B. G. G. Min, H. Guo, S. Kumar, R. H. H. R. H. Hauge, R. E. R. E. E. Smalley and T. V. V. Sreekumar, *Adv. Mater.*, **16**, 58 (2004).
10. J. J. Ge, H. Hou, Q. Li, M. J. Graham, A. Greiner, D. H. Reneker, F. W. Harris and S. Z. D. Cheng, *J. Am. Chem. Soc.*, **126**, 15754 (2004).
11. T. Pirzada, S. A. Arvidson, C. D. Saquing, S. S. Shah and S. A. Khan, *Langmuir*, **30**, 15504 (2014).
12. L. Ji and X. Zhang, *Mater. Lett.*, **62**, 2165 (2008).
13. H. R. Jung, D. H. Ju, W. J. Lee, X. Zhang and R. Kotek, *Electrochim. Acta.*, **54**, 3630 (2009).
14. J. P. Yang, Z. K. Chen, G. Yang, S. Y. Fu and L. Ye, *Polymer (Guildf)*, **49**, 3168 (2008).
15. S. Von Wroblewski, *Ann. Phys. u Chem.*, **8**, 29 (1879).
16. V. Srivastava, D. Gusain and Y. C. Sharma, *Ceram. Int.*, **39**, 9803 (2013).
17. C. L. Wu, M. Q. Zhang, M. Z. Rong and K. Friedrich, *Compos. Sci. Technol.*, **65**, 635 (2005).
18. C. L. Chiang, R. C. Chang and Y. C. Chiu, *Thermochim. Acta.*, **453**, 97 (2007).
19. N. Setoodeh, P. Darvishi and A. Lashanizadegan, *J. Dispers. Sci. Technol.*, **39**, 711 (2017).
20. N. Setoodeh, P. Darvishi and A. Lashanizadegan, *J. Dispers. Sci. Technol.*, **39**, 452 (2017).
21. J. Potreck, K. Nijmeijer, T. Kosinski and M. Wessling, *J. Membr. Sci.*, **338**, 11 (2009).
22. J. A. Barrie and M.-B. Haegg, Membranes in gas separation, in: 4th BOC Priest. Conf., 89 (1986).
23. T. C. Merkel, V. I. Bondar, K. Nagai, B. D. Freeman and I. Pinnau, *J. Polym. Sci. Part B Polym. Phys.*, **38**, 415 (2000).
24. M. Mulder, Basic principles of membrane technology, Kluwer Academic Publishers, London (1996).
25. V. Barbi, S. S. Funari, R. Gehrke, N. Scharnagl and N. Stribeck, *Macromolecules*, **36**, 749 (2003).
26. S. J. Metz, M. H. V. Mulder and M. Wessling, *Film*, **37**, 4590 (2004).
27. T. Watari, H. Y. Wang, K. Kuwahara, K. Tanaka, H. Kita and K. Okamoto, *J. Membr. Sci.*, **219**, 137 (2003).
28. J. S. Chiou and D. R. Paul, *Ind. Eng. Chem. Res.*, **27**, 2161 (1988).
29. G. Chen, X. Zhang, J. Wang and S. Zhang, *J. Appl. Polym. Sci.*, **106**, 3179 (2007).
30. H. Lin, S. M. Thompson, A. Serbanescu-Martin, J. G. Wijmans,

K. D. Amo, K. A. Lokhandwala and T. C. Merkel, *J. Membr. Sci.*, **413-414**, 70 (2012).

31. F. H. Akhtar, M. Kumar and K.-V. Peinemann, *J. Membr. Sci.*, **525**, 187 (2016).

32. F. K. Ko and Y. Wan, Introduction to nanofiber materials, Cambridge University Press, New York (2014).

33. X. Wang, X. Chen, K. Yoon, D. Fang, B. S. Hsiao and B. Chu, *Environ. Sci. Technol.*, **39**, 7684 (2005).

34. K. Yoon, K. Kim, X. Wang, D. Fang, B. S. Hsiao and B. Chu, *Polymer (Guildf)*, **47**, 2434 (2006).

35. D. R. Phillip Gibson, H. L. Schreuder-Gibson, P. Gibson, H. Schreuder-Gibson and D. Rivin, *Colloids Surfaces A Physicochem.*, **188**, 469 (2001).

36. T. Grafe and K. Graham, Int. Nanowovens Tech. Conf., 24 (2002).

37. R. S. Barhate and S. Ramakrishna, *J. Membr. Sci.*, **296**, 1 (2007).

38. R. Huizing, W. Mérida and F. Ko, *J. Membr. Sci.*, **461**, 146 (2014).

39. S. J. Poormohammadian, P. Darvishi and A. M. G. Dezfuli, *Chin. J. Chem. Eng.*, **27**, 100 (2018).

40. S. J. Metz, W. Vandeven, J. Potreck, M. H. V. Mulder, M. Wessling, W. J. C. van de Ven and J. Potreck, *J. Membr. Sci.*, **251**, 29 (2005).

41. S. J. Metz, W. J. C. Van De Ven, M. H. V. Mulder and M. Wessling, *J. Membr. Sci.*, **266**, 51 (2005).

42. M. B. Satterfleld and J. B. Benziger, *J. Phys. Chem. B.*, **112**, 3693 (2008).

43. L. Ji, C. Saquing, SA. Khan and X. Zhang, *Nanotechnology*, **19**, 85605 (2008).

44. M.-J. Wang, S. Wolff and J.-B. Donnet, *Rubber Chem. Technol.*, **64**, 714 (1991).

45. K. M. Sawicka and P. Gouma, *J. Nanoparticle Res.*, **8**, 769 (2006).

46. J. Gao, T. Gao and M. J. Sailor, *Appl. Phys. Lett.*, **77**, 901 (2000).

47. H. Nagel and R. Hezel, *Sol. Energy Mater. Sol. Cells*, **65**, 71 (2001).

48. P. Rittigstein, R. D. Priestley, L. J. Broadbelt and J. M. Torkelson, *Nat. Mater.*, **6**, 278 (2007).

49. P. Roy, D. Kim, K. Lee, E. Spiecker and P. Schmuki, *Nanoscale*, **2**, 45 (2010).

50. A. L. Linsebigler, G. Lu and J. T. Yates, *Chem. Rev.,* **95**, 735 (1995).

51. A. Fujishima and K. Honda, *Nature*, **238**, 37 (1972).

52. X. Wang, M. Fujimaki and K. Awazu, *Opt. Express.*, **13**, 1486 (2005).

53. H. M. Kim, F. Miyaji, T. Kokubo and T. Nakamura, *J. Biomed. Mater. Res.*, **32**, 409 (1996).

54. D. Álvarez, X. R. Nóvoa and C. Pérez, *Prog. Org. Coatings*, **96**, 3 (2015).

55. D. Wang and G. Bierwagen, *Prog. Org. Coatings*, **64**, 327 (2009).

56. H. Lin, S. M. Thompson, A. Serbanescu-Martin, J. G. Wijmans, K. D. Amo, K. A. Lokhandwala, B. T. Low and T. C. Merkel, *J. Membr. Sci.*, **432**, 106 (2013).

57. P. G. Ingole, M. I. Baig, W. K. Choi and H. K. Lee, *J. Mater. Chem. A.*, **4**, 5592 (2016).

58. R. Xing, Y. Rao, W. TeGrotenhuis, N. Canfield, F. Zheng, D. W. Winiarski and W. Liu, *Chem. Eng. Sci.*, **104**, 596 (2013).

59. P. K. Baumgarten, *J. Colloid Interface Sci.*, **36**, 71 (1971).

60. J. Doshi and D. H. Reneker, *Sect. Title Text. Fibers*, **35**, 151 (1995).

61. H. Fong, I. Chun and D. H. Reneker, *Polymer*, **40**, 4585 (1999).

62. J. Deitzel, J. Kleinmeyer, D. Harris and N. C. Beck Tan, *Polymer*, **42**, 261 (2001).

63. M. M. Demir, I. Yilgor, E. Yilgor and B. Erman, *Polymer*, **43**, 3303 (2002).

64. J. J. Van Franeker, M. Turbiez, W. Li, M. M. Wienk and R. A. J. Janssen, *Nat. Commun.*, **6**, 6229 (2015).

65. W. Stöber, A. Fink and E. Bohn, *J. Colloid Interface Sci.*, **26**, 62 (1968).

66. S. Sakka, SoleGel Process and Applications, in: *Handb. Adv. Ceram. Mater. Appl. Process. Prop.*, 883 (2013).

67. R. W. Baker, Membrane Technology and Applications, Wiley, New York (2004).

68. Y. Shen and A. C. Lua, *Chem. Eng. J.*, **188**, 199 (2012).

69. A. Bondi, *J. Phys. Chem.*, **68**, 441 (1964).

70. Y. H. Zhao, M. H. Abraham and A. M. Zissimos, *J. Org. Chem.*, **68**, 7368 (2003).

71. A. Jomekian, R. M. Behbahani, T. Mohammadi and A. Kargari, *Korean J. Chem. Eng.*, **34**, 440 (2017).

72. V. I. Bondar, B. D. Freeman and I. Pinnau, *J. Polym. Sci. Part B Polym. Phys.*, **37**, 2463 (1999).

73. J. H. Kim and Y. M. Lee, *J. Membr. Sci.*, **193**, 209 (2001).

74. A. Khosravi, M. Sadeghi, H. Z. Banadkohi and M. M. Talakesh, *Ind. Eng. Chem. Res.*, **53**, 2011 (2014).

75. C. G. Ma, M. Z. Rong, M. Q. Zhang and K. Friedrich, *Polym. Eng. Sci.*, **45**, 529 (2005).

76. G. Choudalakis and A. D. Gotsis, *Curr. Opin. Colloid Interface Sci.*, **17**, 132 (2012).

77. V. I. Bondar, B. D. Freeman and I. Pinnau, *J. Polym. Sci. Part B Polym. Phys.*, **38**, 2051 (2000).

78. K. L. Wang, S. H. Mccrayb, D. D. Newboldb and E. L. Cussler, *J. Membr. Sci.*, **72**, 231 (1992).

79. R. W. Baker, Membrane Technology and Applications, Wiley, New York (2012).

80. T. C. Merkel, V. Bondar, K. Nagai and B. D. Freeman, *J. Polym. Sci. Part B Polym. Phys.*, **38**, 273 (2000).

81. A. Gabelman and S.-T. Hwang, *J. Membr. Sci.*, **159**, 61 (1999).

82. W. J. Massman, *Atmos. Environ.*, **32**, 1111 (1998).

83. G. Q. Chen, C. A. Scholes, G. G. Qiao and S. E. Kentish, *J. Membr. Sci.*, **379**, 479 (2011).

84. W. Yave, S. Shishatskiy, V. Abetz, S. Matson, E. Litvinova, V. Khotimskiy and K. V. Peinemann, *Macromol. Chem. Phys.*, **208**, 2412 (2007).

85. M. S. A. Wahab and A. R. Sunarti, *Membr. Sci. Technol.*, **2**, 78 (2015).

86. M. S. Jay and M. K. Tripodi, *J. Membr. Sci.*, **8**, 233 (1981).

87. J. Wijmans, A. Athayde and R. Daniels, *J. Membr. Sci.*, **109**, 135 (1996).

88. K. Kneifel, S. Nowak, W. Albrecht, R. Hilke, R. Just and K. V. Peinemann, *J. Membr. Sci.*, **276**, 241 (2006).

89. M. Basafa and M. Pourafshari Chenar, *Sep. Sci. Technol.*, **49**, 2465 (2014).

90. P. D. Dalton, D. Klee and M. Möller, *Polymer (Guildf)*, **46**, 611 (2005).

91. R. Khajavi and M. Abbasipour, *Sci. Iran.*, **19**, 2029 (2012).